ACS Chemical Neuroscience

Letter

pubs.acs.org/chemneuro

Single-Quantum-Dot Tracking Reveals Altered Membrane Dynamics of an Attention-Deficit/Hyperactivity-Disorder-Derived Dopamine Transporter Coding Variant

Oleg Kovtun,[†,§] Dhananjay Sakrikar,[‡] Ian D. Tomlinson,[†] Jerry C. Chang,[∥] Xochitl Arzeta-Ferrer,[†] Randy D. Blakely,[‡,⊥,#] and Sandra J. Rosenthal*[,†,‡,@,▽,○,◆]

[†]Departments of Chemistry and [‡]Pharmacology, Vanderbilt University, Nashville, Tennessee 37235, United States

[§]McCoy & McCoy Laboratories, Inc, Madisonville, Kentucky 42431, United States

[∥]Laboratory of Molecular and Cellular Neuroscience, The Rockefeller University, New York, New York 10065, United States

[⊥]Departments of Psychiatry, [#]Silvio O. Conte Center for Neuroscience Research, [@]Chemical and Biomolecular Engineering, [▽]Physics and Astronomy, and [○]Vanderbilt Institute of Nanoscale Science and Engineering, Vanderbilt University, Nashville, Tennessee 37235, United States

[◆]Materials Science and Technology Division, Oak Ridge National Laboratory, Oak Ridge, Tennessee 37831, United States

Supporting Information

ABSTRACT: The presynaptic, cocaine- and amphetamine-sensitive dopamine (DA) transporter (DAT, *SLC6A3*) controls the intensity and duration of synaptic dopamine signals by rapid clearance of DA back into presynaptic nerve terminals. Abnormalities in DAT-mediated DA clearance have been linked to a variety of neuropsychiatric disorders, including addiction, autism, and attention deficit/hyperactivity disorder (ADHD). Membrane trafficking of DAT appears to be an important, albeit incompletely understood, post-translational regulatory mechanism; its dysregulation has been recently proposed as a potential risk determinant of these disorders. In this study, we demonstrate a link between an ADHD-associated DAT mutation (Arg615Cys, R615C) and variation on DAT transporter cell surface dynamics, a combination only previously studied with ensemble biochemical and optical approaches that featured limited spatiotemporal resolution. Here, we utilize high-affinity, DAT-specific antagonist-conjugated quantum dot (QD) probes to establish the dynamic mobility of wild-type and mutant DATs at the plasma membrane of living cells. Single DAT-QD complex trajectory analysis revealed that the DAT 615C variant exhibited increased membrane mobility relative to DAT 615R, with diffusion rates comparable to those observed after lipid raft disruption. This phenomenon was accompanied by a loss of transporter mobilization triggered by amphetamine, a common component of ADHD medications. Together, our data provides the first dynamic imaging of single DAT proteins, providing new insights into the relationship between surface dynamics and trafficking of both wild-type and disease-associated transporters. Our approach should be generalizable to future studies that explore the possibilities of perturbed surface DAT dynamics that may arise as a consequence of genetic alterations, regulatory changes, and drug use that contribute to the etiology or treatment of neuropsychiatric disorders.

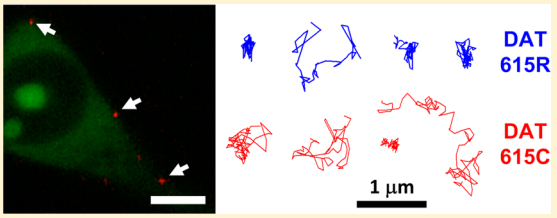

KEYWORDS: *Attention deficit/hyperactivity disorder, amphetamine, cocaine, dopamine transporter, single quantum dot tracking, membrane dynamics*

The high-affinity dopamine (DA) transporter protein (DAT) plays a critical role in maintaining coordinated, dopamine-mediated signaling in the central nervous system (CNS).[1−6] DAT controls the intensity and duration of dopamine signals by reducing the extracellular concentrations of the neurotransmitter through reuptake into presynaptic nerve terminals (Figure 1A). Dysfunction and/or polymorphisms in DAT have been linked to a variety of brain disorders, including schizophrenia, bipolar disorder, dystonia, Parkinson's disease, and attention-deficit/hyperactivity disorder.[3−10] In addition, DAT is a major target for the widely abused psychostimulants, cocaine, a competitive DAT antagonist, and amphetamine, a DA-like substrate with the added ability to trigger reverse DA transport, also a component of commonly prescribed ADHD medications (Figure 1A).[6] DAT has been shown to be tightly regulated through multiple mechanisms, including phosphorylation, protein−protein interactions and membrane trafficking, which can be influenced by psychoactive drugs.[11−23] Over the past decade, several reports have demonstrated that populations of cell surface DAT molecules are associated with distinct, cholesterol-enriched membrane microdomains, often termed "lipid rafts"[51−53], and can also display cholesterol-dependent lateral diffusion and/or functional states.[18,20,24−27] DAT surface dynamics appear to

Published: March 8, 2015

DOI: 10.1021/cn500202c
ACS Chem. Neurosci. 2015, 6, 526−534

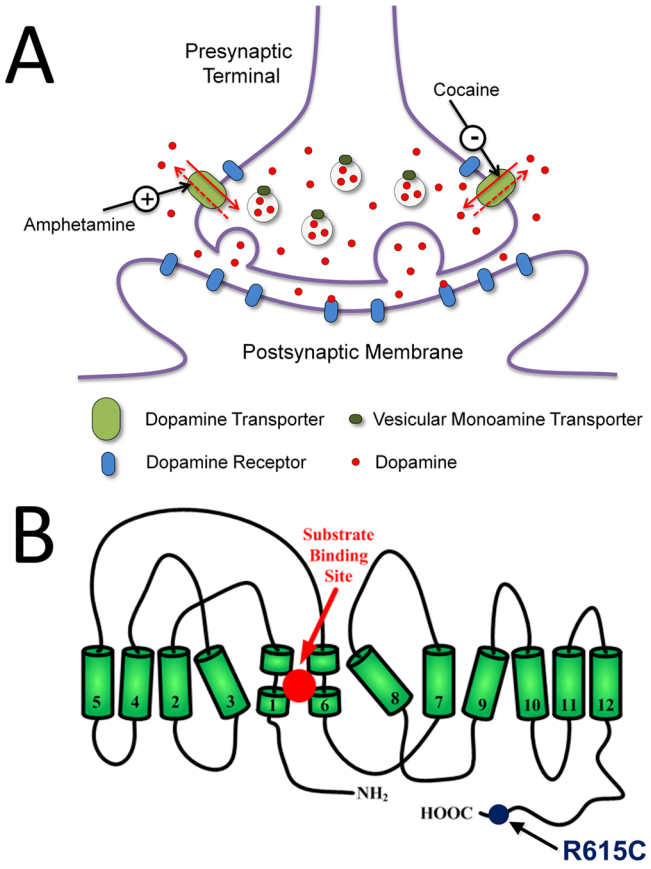

Figure 1. Dopaminergic synapse and dopamine transporter two-dimensional topology. (A) Diagram depicting signal transduction in the dopaminergic synapse. Dopamine is transported within synaptic vesicles and is released by a presynaptic neuron into the synaptic cleft, where it can bind to dopamine receptors on postsynaptic terminals. Normally, dopamine is recycled back into the presynaptic terminal by the dopamine transporter. Cocaine acts as a dopamine transporter antagonist, blocking dopamine reuptake and thereby increasing dopamine synaptic concentration. Amphetamine, on the other hand, depletes synaptic vesicles of dopamine and induces dopamine reverse transport through the dopamine transporter. Amphetamine also binds reversibly to dopamine transporter, slowing dopamine reuptake.(B) A two-dimensional topology of DAT based on the leucine transporter (LeuT) is shown with 12 transmembrane segments, intracellularly oriented N- and C-termini, and substrate binding site. The location of the R615C substitution in a highly conserved region of the transporter's C-terminus is shown. (Reproduced with permission from ref 38. Copyright 2011 American Chemical Society.)

depend both on localization with these membrane microdomains and interactions with intracellular protein networks, which appear to be critical for proper spatiotemporal regulation of DAT function.[11,13−15] Despite the clear clinical importance of understanding DAT modulation, a dearth of information exists that relates alterations in these regulatory mechanisms to a risk for brain disorders. To a significant degree, investigation of these mechanisms has been limited by a reliance on the ensemble-averaging approaches available with conventional biochemical and optical techniques.

Biomolecule detection using quantum dots (QDs), nanometer-sized semiconductor crystals, addresses the limitations associated with population-based optical and biochemical techniques, as QDs offer several key advantages over traditional fluorophores: (i) broad absorption spectra and narrow, Gaussian-like emission spectra (25−40 nm at full-width half-maximum of the emission peak), (ii) high quantum yields and large molar extinction coefficients, (iii) superior resistance to photobleaching, and (iv) versatility of surface functionalization.[28−30,59] Moreover, the use of QDs considerably simplifies the technical requirements for a highly sensitive, single molecule tracking experiments where observation of single QD-labeled targets can be achieved with ∼5−10 nm accuracy overtime periods that range from milliseconds to minutes.[31,32]

The primary focus of our group has been the development of ligand-conjugated QD probes that enable a specific targeting of neuronal membrane proteins, such as the serotonin (5-HT) transporter (SERT), DAT, and the norepinephrine (NE) transporter (NET), as well as the γ-aminobutyric acid (GABA) receptor.[33−41] Several groups have made elegant use of QDs conjugated to surface-epitope directed antibodies to track the lateral mobility and regulation of cell surface receptors and transporters.[60−62] However, since many membrane proteins lack surface-epitope antibodies suitable for dynamic tracking of single molecules, the cornerstone of our probe development has been the QD coupling of high-affinity, small-molecule antagonists that can provide for pseudoirreversible probe binding and the analysis of surface trafficking properties.[39−41] Our approach enables both highly sensitive population detection of transporters and receptors as well as single QD analysis of target protein diffusion dynamics. In the most recent effort, Chang et al. used antagonist-conjugated QD probes in conjunction with high-speed, line-scanning laser confocal microscopy to reveal a connection between receptor-mediated signaling-pathways that alter SERT activity and the membrane dynamics of SERT proteins on the surface of serotonergic cells.[41]

Here we adapted our recently reported, DAT-specific probe IDT444 to establish dynamic imaging of single DAT-QD complexes on the surface of living cells.[38,40] The biotinylated, PEGylated cocaine analogue IDT444 provides for labeling of surface DAT molecules via streptavidin-conjugated QD (SavQD) coupling to DAT-bound ligand and has been shown to bind to DAT with high affinity and excellent specificity.[38] In this study, we extend our efforts to visualize single QD-labeled DAT complexes in living cells, providing for a characterization of their membrane dynamics and their sensitivity to membrane cholesterol extraction, drug impact, and ADHD-derived coding variation.

RESULTS AND DISCUSSION

Tracking Single DAT-QD Complexes. To overcome the limitations of ensemble-averaging and poor spatiotemporal resolution of the currently existing arsenal of DAT probes, we developed a high-affinity, biotin-labeled and DAT-specific cocaine analogue IDT444 that permits pseudoirreversible binding to SavQDs, while retaining high-affinity interactions with DAT.[38,40] The flexible PEG-based linker of IDT444 also reduces potential steric hindrance of QDs with the cell surface in addition to enhancing water solubility of the ligand.[46] With this probe strategy, we demonstrated previously that QD-IDT444 conjugates successfully detected plasma membrane-localized DATs in both transiently and stably transfected expression systems. Importantly, DAT-bound QD-IDT444 conjugates displayed a very slow off-rate (>1 h), allowing for prolonged visualization of surface DAT molecules.[40] In the current study, we implemented our two-step QD labeling strategy to establish, for the first time, the dynamic imaging of

DOI: 10.1021/cn500202c
ACS Chem. Neurosci. 2015, 6, 526−534

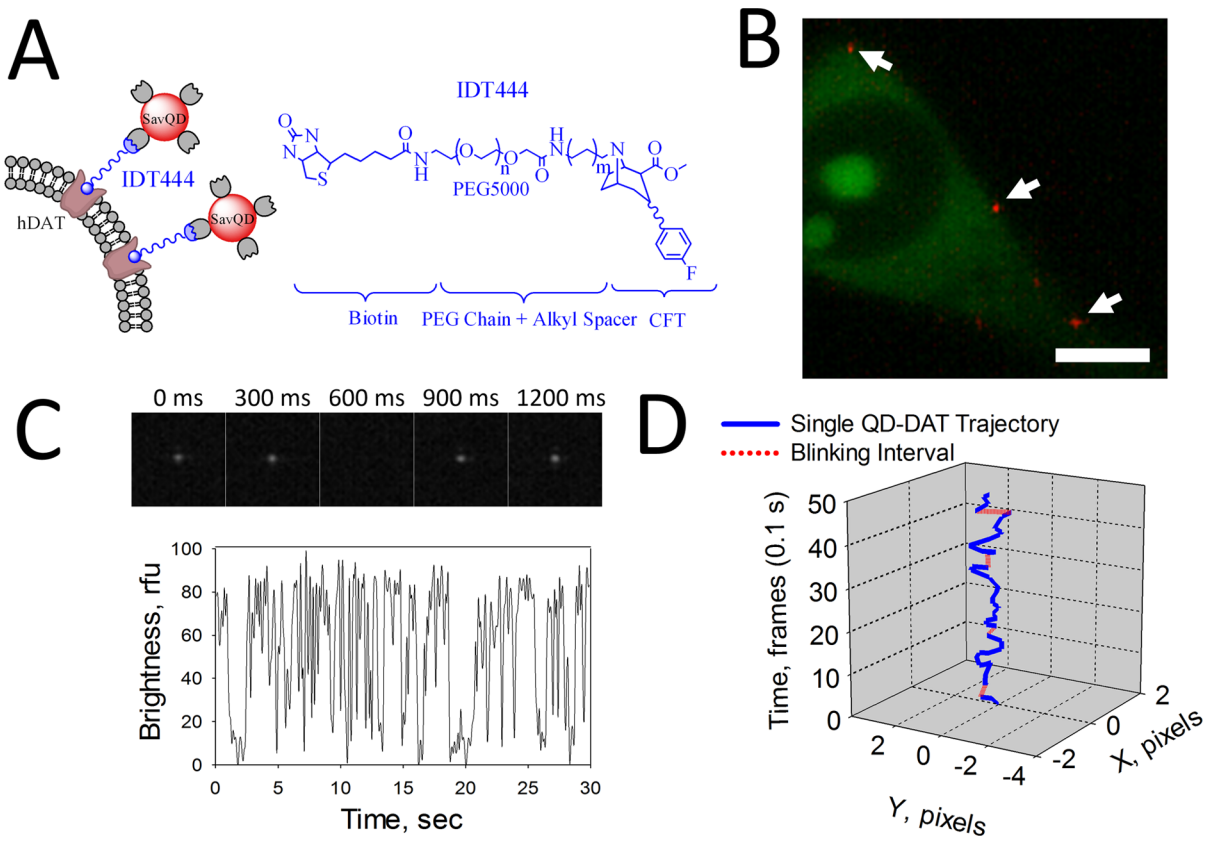

Figure 2. Time-lapse imaging of DAT in the plasma membrane of stably transfected Flp-In 293 cells. (A) Schematic of the QD labeling protocol. DAT-specific IDT444 cocaine analogue accesses the high-affinity binding site of DAT. Its biotin terminus facilitates subsequent DAT recognition with SavQDs. (B) Fluorescence micrograph showing characteristic surface QD labeling of DATs. IDT307, a neurotransmitter mimic, results in intracellular green fluorescence after DAT-mediated transport and was used as a cell position and focal plane gauge. Bar: 5 μm. (C) Representative time-lapse image series of a single SavQD immobilized (spun-cast) on a glass coverslip and a corresponding emission spectrum trace. Emission spectra of single nanocrystals exhibit fluorescence intermittency, a criterion used to distinguish single QDs from aggregation artifacts. (D) An example trajectory of single DAT-QD complex undergoing diffusion in the plasma membrane.

membrane DATs in live cells with single QDs. The two-step labeling approach employed to detect membrane DATs is illustrated in Figure 2A. A representative confocal fluorescence image in Figure 2B depicts individual DAT-QD complexes on the cell surface. Nonspecific QD binding could be virtually eliminated by the inclusion of at least 1% w/w bovine serum albumin (BSA) in the QD imaging buffer. We monitored the movement of QD-labeled DATs in Flp-In 293 cell membranes using time-lapse image acquisition at a scan speed of 10 Hz over 1 min.[41] It should be noted that only cell surface-bound QDs in a focal plane at the membrane-glass interface were detected. To minimize the effects of endocytosis, QD labeling was carried as the last experimental step, and QD-labeled cells were imaged immediately postlabeling. Also, data acquisition was achieved within 10 min of the final wash step. Fluorescence intermittency, an intrinsic property of single nanocrystals, was used as a criterion to ensure analysis of single QD events (Figure 2C).[42−45] An example of a DAT-QD trajectory is shown in blue in Figure 2D, with blinking/off intervals shown in red. To successfully interpolate the position of QDs between frames during which they blinked, IDL-based single tracking algorithms were employed (see Methods).

Attention-Deficit/Hyperactivity-Disorder-Derived DAT Coding Variation Produces Altered Transporter Mobility. Recently, in a screen for DAT coding variants in ADHD subjects, we identified and characterized the rare variant, R615C, where an arginine codon at amino acid 615 amino has been altered to encode cysteine.[27] The 615C variant is located in a highly conserved region of the DAT C-terminus, a region previously implicated in DAT trafficking regulation (Figure 1B).[21,54,55] We found that when DAT 615C is studied in in stably transfected Flp-In 293 cells, the variant transporter displays a loss of DAT trafficking sensitivity to both protein kinase C activation as well as amphetamine treatments.[27] In the same report, we also demonstrated that the DAT 615C variant is hyperphosphorylated and displays altered associations with flotillin- and GM1 ganglioside-enriched membrane microdomains. In the present study, we sought to test the hypothesis that these behaviors may be accompanied by disrupted lateral diffusion, visible with our antagonist-conjugated QD approach. Example time series of Flp-In 293 cells expressing DAT 615R (wildtype) or 615C (mutant) labeled with QDs are shown in Supporting Information Videos 1 and 2, as a single cell and a monolayer cluster of five cells, respectively. Time-lapse images were taken immediately after labeling, using IDT307 to visual the interior of the cells and to rule out endocytosis. Visual inspection indicated that the majority of QD-DATs in both populations remained largely confined over a 1 min time interval. Examples of QD trajectories are shown in Figure 3A. Several trajectories of QDs immobilized on a glass coverslip are shown for comparison (Figure 3A, bottom row). The obtained trajectories were analyzed, and the combined MSD versus time

DOI: 10.1021/cn500202c
ACS Chem. Neurosci. 2015, 6, 526−534

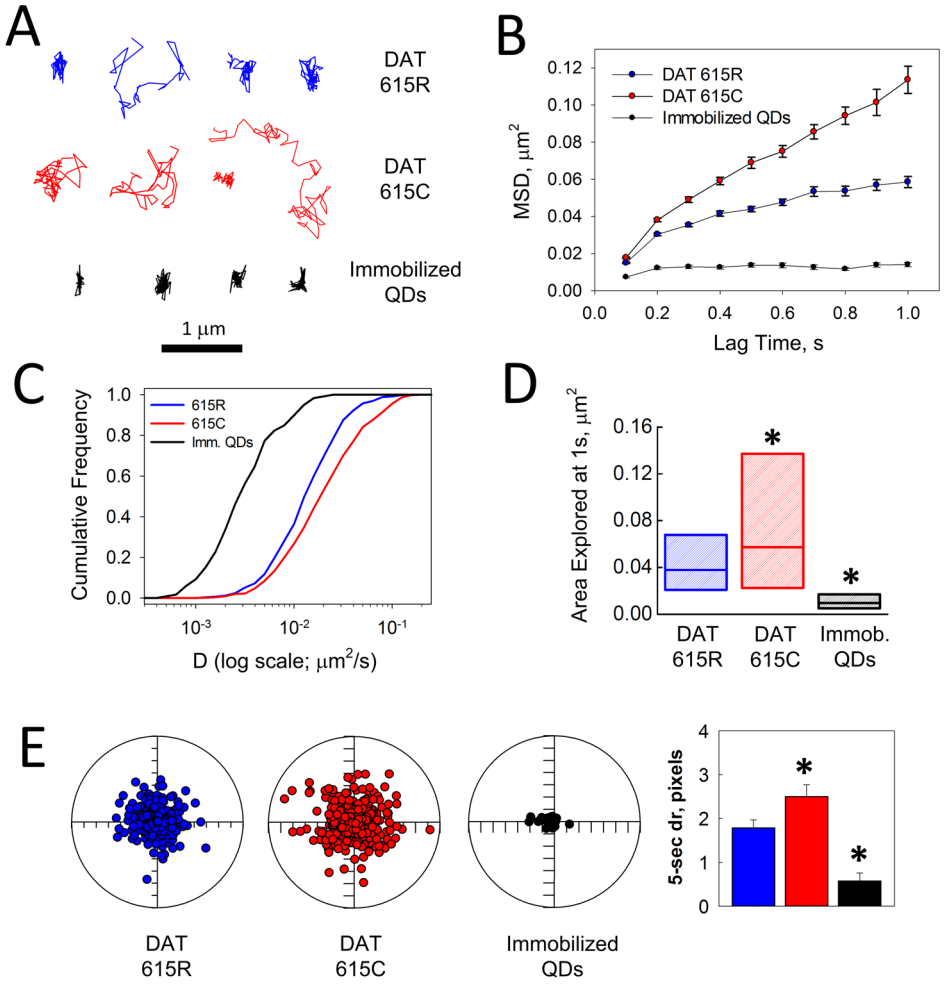

Figure 3. Single-quantum dot tracking of the wildtype DAT 615R variant and the attention deficit/hyperactivity-derived DAT 615C variant in Flp-In 293 cells.(A) Example trajectories of single DAT 615R-QD and DAT 615C-QD complexes ($n \geq 500$ trajectories from at least 20 cells over the course of at least three independent experiments). Trajectories of immobilized QDs on a coverglass (Bottom row) are shown for comparison. (B) Ensemble mean square displacement versus time plots for QD-labeled DAT 615R and DAT 615C in Flp-In 293 cells as well as QDs spin-cast on a coverslip. Error bars indicate SD. (C) Cumulative probability plots depicting diffusion rate distributions (one-way ANOVA with Bonferroni-Dunn's post hoc test on raw diffusion coefficient values: DAT 615R vs DAT 615C, ***$P < 0.001$; DAT615R vs immobilized QDs on a coverslip, ***$P < 0.001$). (D) Explored areas at 1 s, shown as color box plot histograms. Median is represented as a line; color box represents the 25%−75% interquartile range (one-way ANOVA with Bonferroni-Dunn's post hoc test: DAT 615R vs DAT 615C, ***$P < 0.001$; DAT615R vs Immobilized QDs on a coverslip, ***$P < 0.001$). (E) Two-dimensional polar plots of 5 s radial displacements (d_{5s}) of single QD-DAT 615R, QD-DAT 615C, and immobilized QDs normalized to their starting coordinates. Radius of a polar plot is 2.8 μm. Mean d_5 values were compared using one-way ANOVA with Bonferroni-Dunn's post hoc test; ***$P < 0.001$ with respect to QD-DAT 615R. Asterisks in D and E denote $P < 0.001$ statistical significance level.

Table 1. Comparison of Median Diffusion Coefficients and Explored Areas at 1 s of QD-Labeled DAT 615R and DAT 615C Variants under Basal, Methyl-β-cyclodextrin-Treated, and Amphetamine-Treated Conditions in Flp-In 293 Cells[a]

DAT coding variant	experimental conditions	trajectories analyzed	median D, $\mu m^2/s$	median explored area at 1 s, μm^2
615R	basal	584	0.016[0.0095, 0.029]	0.038[0.021, 0.068]
	+ MβCD	251	0.025[0.011, 0.046]	0.052[0.025, 0.12]
	+ AMPH	273	0.020[0.012, 0.046]	0.045[0.024, 0.11]
615C	basal	550	0.024[0.012, 0.049]	0.057[0.023, 0.14]
	+ MβCD	265	0.023[0.012, 0.041]	0.054[0.024, 0.12]
	+ AMPH	259	0.027[0.012, 0.052]	0.060[0.024, 0.15]

[a]Interquartile (25%−75%) range (IQR) associated with each median value is provided in the brackets.

plots for all measured trajectories of QD-DAT615R, QD-DAT-615C, and immobilized QDs are shown in Figure 3B. All MSD plots showed a characteristic confined diffusion curvature in the membrane of Flp-In 293 cells, demonstrated by the downward curve of the slopes compared to the linear slope of data points 2−4. This is in comparison to a linear slope representing random diffusion, and an increased upward slope representing directed diffusion.[48−50] Figure 3C compares the distributions of diffusion coefficients (D_{1-3}) derived from individual MSD versus time plots. The median diffusion coefficient of QD-DAT

DOI: 10.1021/cn500202c
ACS Chem. Neurosci. 2015, 6, 526−534

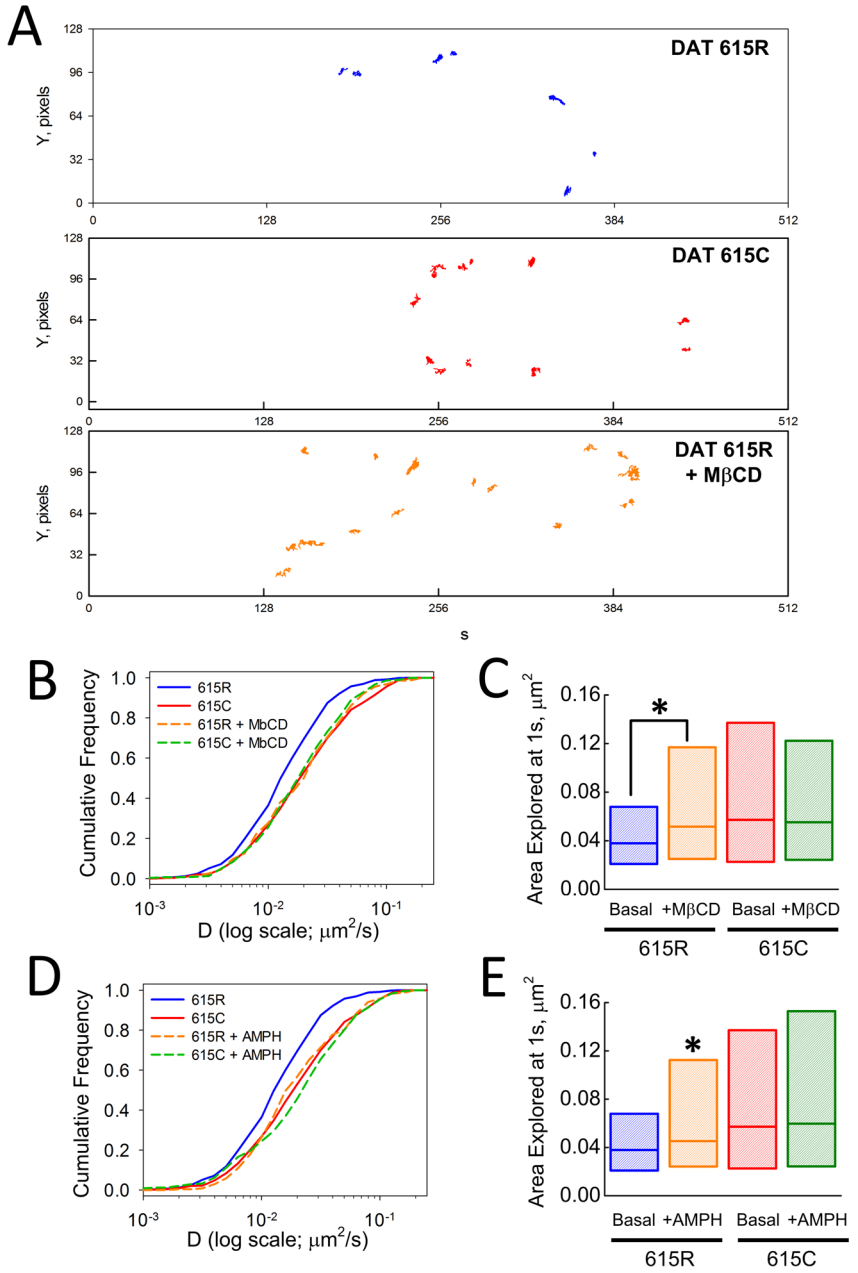

Figure 4. DAT 615R and DAT 615C membrane diffusion after MβCD-mediated cholesterol depletion and amphetamine treatment in Flp-In 293 cells. (A) Example trajectories. Scale: 1 pixel = 200 nm. (B and D) Comparison of diffusion coefficient distributions for single DAT 615R-QDs and DAT 615C-QDs under basal, methyl-β-cyclodextrin-treated, amphetamine-treated conditions (one-way ANOVA with Bonferroni-Dunn's post hoc test on nontransformed data: DAT 615R basal vs DAT 615C basal, ***$P < 0.001$; DAT 615R basal vs DAT 615R + methyl-β-cyclodextrin, ***$P < 0.001$; DAT 615C basal vs DAT 615C + methyl-β-cyclodextrin, $P = 0.4$; DAT 615R basal vs DAT 615R + amphetamine, ***$P < 0.001$; DAT 615C basal vs DAT 615C + amphetamine, $P = 0.2$). (C and E) Comparison of the distributions of explored areas (MSD at 1 s) by single DAT 615R-QDs and DAT 615C-QDs under basal andmethyl-β-cyclodextrin-treated conditions (one-way ANOVA with Bonferroni-Dunn's post hoc test on nontransformed values: DAT 615R basal vs DAT 615C basal, ***$P < 0.001$; DAT 615R basal vs DAT 615R + methyl-β−cyclodextrin, ***$P < 0.001$; DAT 615C basal vs DAT 615C + methyl-β-cyclodextrin, $P = 0.2$). (D) Comparison of the distributions of explored areas (at 1 s) by single DAT 615R-QDs and DAT 615C-QDs under control and amphetamine-treated conditions (one-way ANOVA with Bonferroni-Dunn's post hoc test: DAT 615R basal vs DAT 615C basal, ***$P < 0.001$; DAT 615R basal vs DAT 615R + amphetamine, **$P < 0.01$; DAT 615C basal vs DAT 615C + amphetamine, $P = 0.7$). For each data set, $n \geq 250$ single DAT-QD trajectories from at least three independent experiments. Asterisks in (B) and (C) denote $P < 0.001$ and $P < 0.01$ statistical significance levels, respectively.

615R (wildtype) was 0.016 $\mu m^2/s$ (1.6×10^{-10} cm^2/s), which is consistent with the diffusion coefficient values found for SERT protein,[41] whereas QD-tagged DAT 615C mutants exhibited significantly faster diffusion, with the median diffusion coefficient of 0.024 $\mu m^2/s$ (2.4×10^{-10} cm^2/s) (Table 1, $p < 0.001$, one-way ANOVA with a Bonferroni-Dunn's post hoc test). We then compared the median area explored at 1 s by DAT in the plasma membrane and confirmed that the explored area is significantly larger for the 615C variant (Figure 3D; $p < 0.001$, one-way ANOVA with a Bonferroni-Dunn's post hoc test). Figure 3E shows 5 s displacement vector maps for all QD-DAT 615R and QD-DAT 615C trajectories, with initial QD

DOI: 10.1021/cn500202c
ACS Chem. Neurosci. 2015, 6, 526−534

positions located at the origin. Again, QD-DAT 615C complexes exhibited greater mobility than their QD-DAT 615R counterparts, as indicated by a more scattered distribution and a significantly larger 5 s radial displacement ($p < 0.001$, one-way ANOVA with a Bonferroni-Dunn's post hoc test). Thus, in agreement with our hypothesis, we determined that DAT 615C membrane dynamics were characterized by a significantly faster diffusion rate, a larger explored membrane area at 1s, and a greater mobile fraction under basal conditions. Our data is consistent with altered DAT 615C basal membrane dynamics as contributing to potential functional dysregulation observed with the variant.[27]

DAT-615R and DAT-615C Surface Mobility is Differentially Regulated by Methyl-β-cyclodextrin and Amphetamine. Cholesterol and GM1 ganglioside-rich membrane rafts play a major role in the capacity for DAT regulation, produced both by endogenous signaling pathways and by psychostimulants.[18,20,24] Our prior study using confocal microscopy revealed a significant loss of localization to membrane microdomains, revealed by GM1 labeling with fluorescent cholera toxin B.[27] These findings predict that the DAT 615C variant may display an altered sensitivity to raft disruption, achieved via membrane cholesterol extraction. To examine the effects of membrane raft disruption on DAT lateral mobility, we utilized methyl-β-cyclodextrin, a commonly used cholesterol-extracting agent. Previously, we demonstrated that methyl-β-cyclodextrin treatment of SERT-expressing RN46A cells results in a disruption of GM1 positive membrane microdomains and an increase in the lateral mobility of Qdot-tagged SERT proteins.[41] Additionally, Adkins et al. were able to mobilize a fraction of cell surface DAT molecules after membrane raft disruption with 10 mM methyl-β-cyclodextrin, as measured using ensemble-averaged fluorescence recovery after photobleaching (FRAP).[24] To investigate this possibility at the single molecule level, we treated DAT 615R- and DAT 615C- expressing Flp-In 293 cells with 5 μM methyl-β-cyclodextrin for 30 min, performed the two-step QD labeling protocol, and then acquired confocal time-lapse images (note that the concentration of methyl-β-cyclodextrin used is lower than Sakrikar et al. due to potential morphology changes seen with higher doses.) Wild-type DAT 615R mobility after membrane raft disruption was characterized by a significantly greater diffusion coefficient with a larger explored area when compared with untreated cells (Table 1; Figure 4; $p < 0.001$, one-way ANOVA with a Bonferroni-Dunn's post hoc test). In contrast, methyl-β-cyclodextrin treatment failed to enhance the mobility of DAT 615C (Figure 4B and C; $p > 0.05$, one-way ANOVA with a Bonferroni-Dunn's *post hoc* test), supporting the hypothesis that the variant transporter's functional and regulatory disturbance arises from its mislocalization to a compartment where cholesterol content is not a determinant of the transporter's lateral mobility. The decreased localization of DAT 615C in membrane domains is consistent with previous findings with mutations of the carboxyl terminus.[23] Interestingly, as we previously demonstrated that DAT 615C exhibits constitutive endocytosis and recycling, as compared with the highly regulated intracellular trafficking of DAT 615R, our findings support the idea that membrane compartmentalization is critical for normal DAT regulation and that risk for DA-related disorders, here modeled with a genetic variant linked to ADHD, may arise in some individuals as a result of DAT mistargeting to these domains.

In our initial studies, we also demonstrated that the DAT 615C variant exhibits hyperphorsphorylation and a marked insensitivity to amphetamine-induced trafficking.[27] Amphetamine treatments evoke both an acute translocation of DAT to the cell surface, seconds after exposure, or cause DAT internalization after minutes of amphetamine treatment.[17,22,27] Our visualization methods, implemented over a millisecond to seconds time scale, should not be influenced by rapid membrane insertion events as QD labeling is restricted to proteins labeled at the cell surface. Thus, we treated DAT 615R- and DAT 615C-expressing Flp-In 293 cells with 10 μM amphetamine for 30 min and then exposed cells to the two-step QD labeling protocol.

Using real-time single-particle trajectory analysis, we observed a significant increase to the lateral membrane mobility of wild-type DAT 615R when treated with amphetamine (Table 1; Figure 4D, E; $p < 0.001$, one-way ANOVA with a Bonferroni-Dunn's post hoc test). This is supported by Rao et al. in which ensemble-averaged florescence recovery using AlexaFluor488-DAT demonstrated increased lateral mobility in filopodia of postnatal DA neurons after 60 μM amphetamine treatment for 30 min.[56] We also demonstrate that DAT 615C proteins are already as mobile as the amphetamine treated wild-type DAT, and that addition of amphetamine does not result in additional elevations in DAT 615C lateral membrane mobility ($p > 0.05$, one-way ANOVA with a Bonferroni-Dunn's post hoc test). In addition, as stated previously, DAT 615C also shows no increase in membrane mobility upon disruption of cholesterol with MβCD. It has been hypothesized that the amphetamine-induced increase in DAT mobility is attributed to calcium/calmodulin-dependent protein kinase II-mediated phosphorylation of the DAT N-terminus.[56] This is consistent with our single-particle trajectory analysis, as the DAT 615C variant demonstrates basal hyperphosphorylation of the N-terminus.[16,27] We suspect that our data indicates a mislocalization the variant transporter to membrane domains lacking normal protein associations that restrict lateral mobility. DAT hyperphosphorylation may either drive transporter mislocalization or arise from mislocalization away from compartments that restrict phosphorylation (e.g., the presence of DAT phosphatases). Further studies are warranted that explore the spatial segregation of DAT post-translational modifications in the context of the DAT 615C mutation.

■ SUMMARY AND CONCLUSIONS

An important goal of this study was to establish a generalizable strategy for evaluation of the plasma membrane dynamics of the cocaine- and amphetamine-sensitive DAT protein with the nanometer resolution required to monitor transporters localized to membrane subdomains. Our single QD-based imaging approach enabled us, for the first time, to detect the lateral mobility of individual DAT-QD complexes in living cells. Using this approach, we were able to assess transporter responses to microdomain destabilization, a disease-associated mutation, and an addictive psychostimulant also used in the treatment of ADHD. Real-time, single DAT-QD trajectory analysis revealed that plasma membrane dynamics of the ADHD-associated DAT 615C coding variant exhibit a significantly higher diffusion rate, a larger explored membrane area, and a greater mobile fraction under basal conditions. In response to cholesterol extraction and amphetamine stimulation, single DAT 615C molecules fail to exhibit altered mobility, consistent with the transporter's surface mislocaliza-

DOI: 10.1021/cn500202c
ACS Chem. Neurosci. 2015, 6, 526−534

tion and consequent elevation in basal mobility. We hypothesize that the higher basal mobility of the mutant transporter reflects an untethering of the variant transporter from regulated protein associations normally acquired by transporter localization to cholesterol/GM-1 enriched membrane microdomains. Further use of our approach should allow for an analysis of DAT regulatory proteins, providing additional clues to DA regulatory perturbations that can add further support for DA-linked neuropsychiatric disorders.

METHODS

Materials. DMEM, FBS, hygromycin B, AMP QDs, and SavQDs (emission max at 655 nm) were from Life Technologies. Amphetamine, methyl-β-cyclodextrin, poly-D-lysine, and BSA were purchased from Sigma-Aldrich. Four-well chambered cover glass dishes were purchased from Lab-Tek. IDT307 (APP+, 4-(4-dimethylamino)-phenyl-1-methylpyridinium iodide) and IDT444 were synthesized as previously described.[35]

Cell Culture, Transfections, and Stable Cell Line Generation. Flp-In 293 cells were used to generate stable lines expressing either DAT 615R or DAT 615C following the manufacturer's protocol (Life Technologies). Flp-In 293 cell line is designed for rapid generation of stable cell lines that ensure high level expression of the protein of interest from a Flp-In expression vector. These cells contain a single stably integrated FRT site at a transcriptionally active genomic locus. Targeted integration of a Flp-In expression vector ensures high-level expression of the gene of interest. The Flp-In 293 host cell line (Invitrogen) was grown in complete medium (DMEM with 2 mM/L glutamine, 10% FBS, 1% pen/strep) in a 37 °C incubator with 5% CO_2. The wild-type or mutant human DAT (hDAT) cDNA cloned in the pcDNA5/FRT expression vector was transfected into Flp-In-293 cells using the Fugene 6 transfection reagent (Roche, NJ). After 48 h recovery, the cells were grown in medium with 100 μg/mL hygromycin B added for several weeks to select for resistant cells where the cDNA construct had been recombined into the Flp-In site, meaning that a minimum overexpression of the protein was consistent through the cell lines in the Flp-In-293 cells.[27]

QD Labeling of DAT-Expressing Flp-In 293 Cells. DAT 615R- or DAT 615C-expressing cells were seeded in poly-D-lysine coated Lab-Tek slides and grown for 24 h. QD labeling was implemented via a two-step protocol. Cells were washed twice with warm Krebs'–Ringer's–HEPES (KRH) (130 mM NaCl, 1.3 mM KCl, 2.2 mM $CaCl_2$, 1.2 mM $MgSO_4$, 1.2 mM KH_2PO_4, 10 mM HEPES,pH 7.4) buffer and incubated with a subsaturating IDT444 concentration of 10 nM in KRH at 37 °C and 5% CO_2. Following two washes with warm KRH, cells were then incubated with a 50 pM dose of SavQDs in warm phenol red-free DMEM/2% bovine serum albumin (imaging buffer), washed three times with warm imaging buffer, and used for time-lapse image series acquisition. To perform cholesterol depletion, methyl-β-cyclodextrin was added to Flp-In 293 cells to a final concentration of 5 μM (30 min incubation at 37 °C and 5% CO_2). Cells were then washed three times with warm KRH, subjected to the QD labeling protocol, and imaged. Amphetamine was administered in an analogous way, with a final effective dose of 10 μM (20 min incubation at 37 °C and 5% CO_2). Amphetamine-treated cells were washed three times with warm KRH, subjected to the QD labeling protocol, and imaged in the presence of 10 μM amphetamine.

High-Speed Confocal Microscopy. For high speed line-scanning confocal microscopy, images were obtained on a Zeiss LSM 5 Live confocal system and viewed with a Zeiss 63×/1.4 NA oil immersion objective lens. Excitation was provided by a 488 nm 100 mW diode laser. Imaging was performed at 37 °C. QD fluorescence was collected using a long pass 650 filter. Single QD tracking was performed at a scan rate of 10 Hz for 1 min. Data were obtained within 10 min of the final wash step after QD labeling.

Data Analysis. Individual TIFF (tagged image file format) images were extracted from sequence files and recompiled as 8-bit image stacks by using ImageJ (National Institutes of Health, Bethesda, MD). Image analysis and trajectory construction were performed using IDL software (Research Systems, Boulder, CO) with algorithms available as shareware at http://www.physics.emory.edu/faculty/weeks/. The localization accuracy of the central position of the QD in our imaging approach was estimated to be ±10−15 nm.[47] The uncertainty of the fitted coordinate was estimated ($\Delta\sigma$) via $\Delta\sigma \approx w/\mathrm{SNR}$ (nm), where w (width) is approximately equal to the wide-field diffraction limit (which for visible light is about 250 nm) and SNR is signal-to-noise ratio defined as $\mathrm{SNR} = I_0/(\sigma_{bg}^2 + \sigma_{I0}^2)^{1/2}$, where I_0 is the maximum signal intensity above background, σ_{bg}^2 is the variance of the background intensity values, and σ_{I0}^2 is the variance of the maximum signal intensity above the background. Intermittency of QD fluorescence was used to verify that single fluorophores were analyzed, and extracted trajectories were at least 5 s in length. Trajectories were considered continuous if a blinking QD was rediscovered within a 3-pixel radius and 10-frame window. For each trajectory, mean square displacement (MSD), $r^2(t)$, was computed as follows:

$$\langle r^2(n\delta t)\rangle = \frac{1}{N-n}\sum_{j=0}^{N-n-1}\{[x(j\delta t + n\delta t) - x(j\delta t)]^2 + [y(j\delta t + n\delta t) - y(j\delta t)]^2\} \quad (n = 0, 1, 2, ..., N-1) \qquad (1)$$

where δt is the temporal resolution of the acquisition device, $(x(j\delta t), x(j\delta t))$ is the particle coordinate at $t = j\delta t$, and N is the number of total frames recorded for an individual particle. The median MSD (at $t = 1$ s) of the QD population represents the area explored within 1 s. Individual microscopic diffusion coefficient D was determined by fitting the first 1−3 points of the MSD versus time curves with the equation:

$$r^2(t)_{1-3} = 4D_{1-3}t + \text{offset} \qquad (2)$$

This fit is generally used because it determines D independently of the type of motion.[57,58] The distribution of explored area (at $t = 1$ s) was represented as box plot histograms with median, 25% and 75% interquartiles, and the distribution of D_{1-3}-values for each experimental condition was displayed as cumulative probability histograms. Statistical significance of differences in median values was determined using the one-way ANOVA with Bonferroni-Dunn's post hoc test on nontransformed values.

ASSOCIATED CONTENT

Supporting Information

Example time-lapse image series demonstrating diffusion of immobilized QDs as well as QD-DAT 615R and QD-DAT 615C complexes on the surface of Flp-In 293 cells. This material is available free of charge via the Internet at http://pubs.acs.org.

AUTHOR INFORMATION

Corresponding Author

*E-mail: sandra.j.rosenthal@vanderbilt.edu.

Funding

This work was supported by NIH Grants EB003728 to S.J.R. and MH094527 to R.D.B.

Notes

The authors declare no competing financial interest.

ACKNOWLEDGMENTS

The authors thank Dr. Sam Wells of the VU Cell Imaging Shared Resource for his assistance with confocal microscopy. Confocal imaging using Zeiss LSM 5 Live was performed in part through the use of the VUMC Cell Imaging Shared Resource supported by NIH Grants CA68485, DK20593, DK58404, HD15052, DK59637, and EY08126.

DOI: 10.1021/cn500202c
ACS Chem. Neurosci. 2015, 6, 526−534

■ ABBREVIATIONS

ADHD, attention deficit/hyperactivity disorder; AMPH, amphetamine; BSA, bovine serum albumin; CaMKII, calcium/calmodulin-dependent protein kinase II; DA, dopamine; DAT, dopamine transporter; DAT 615R, wildtype DAT coding variant; DAT 615C, ADHD-derived DAT R615C coding variant; MβCD, methyl-β-cyclodextrin; PKC, protein kinase C; QD, quantum dot; SavQD, streptavidin-conjugated QD; SQDT, single-quantum dot tracking

■ REFERENCES

(1) Giros, B., Giros, B., and Caron, M. G. (1993) Molecular characterization of the dopamine transporter. *Trends Pharmacol. Sci. 14* (2), 43−49.

(2) Bannon, M. J. (2004) Dopamine. *Nature Encyclopedia of Life Sciences*, Nature Publishing Group, New York, retrieved May 6, 2010 from www.els.net.

(3) Giros, B., Jaber, M., Jones, S. R., Wightman, R. M., and Caron, M. G. (1996) Hyperlocomotion and indifference to cocaine and amphetamine in mice lacking the dopamine transporter. *Nature 379* (6566), 606−612.

(4) Raul, R. G., Sara, R. J., and Marc, G. C. (1999) Functional hyperdopaminergia in dopamine transporter knock-out mice. *Biol. Psychiatry 46* (3), 303−311.

(5) Ralph, R. J., Paulus, M. P., Fumagalli, F., Caron, M. G., and Geyer, M. A. (2001) Prepulse Inhibition Deficits and Perseverative Motor Patterns in Dopamine Transporter Knock-Out Mice: Differential Effects of D1 and D2 Receptor Antagonists. *J. Neurosci. 21* (1), 305−313.

(6) Schmitt, K. C., and Reith, M. E. A. (2010) Regulation of the dopamine transporter. *Ann. N. Y. Acad. Sci. 1187*, 316−340.

(7) Greenwood, T. A., Alexander, M., Keck, P. E., McElroy, S., Sadovnick, A. D., Remick, R. A., and Kelsoe, J. R. (2001) Evidence for linkage disequilibrium between the dopamine transporter and bipolar disorder. *Am. J. Med. Genet. 105* (2), 145−151.

(8) Swanson, J. M., Flodman, P., Kennedy, J., Spence, M. A., Moyzis, R., Schuck, S., Murias, M., Moriarity, J., Barr, C., Smith, M., and Posner, M. (2000) Dopamine genes and ADHD. *Neurosci. Biobehav. Rev. 24* (1), 21−25.

(9) Kirley, A., Lowe, N., Hawi, Z., Mullins, C., Daly, G., Waldman, I., McCarron, M., O'Donnell, D., Fitzgerald, M., and Gill, M. (2003) Association of the 480 bp DAT1 allele with methylphenidate response in a sample of Irish children with ADHD. *Am. J. Med. Genet., Part B 121B* (1), 50−54.

(10) Kurian, M. A., Zhen, J., Cheng, S.-Y., Li, Y., Mordekar, S. R., Jardine, P., Morgan, N. V., Meyer, E., Tee, L., Pasha, S., Wassmer, E., Heales, S. J. R., Gissen, P., Reith, M. E. A., and Maher, E. R. (2009) Homozygous loss-of-function mutations in the gene encoding the dopamine transporter are associated with infantile parkinsonism-dystonia. *J. Clin. Invest. 119* (6), 1595−1603.

(11) Eriksen, J., Jorgensen, T. N., and Gether, U. (2010) Regulation of dopamine transporter function by protein-protein interactions: new discoveries and methodological challenges. *J. Neurochem. 113* (1), 27−41.

(12) Cremona, M. L., Matthies, H. J. G., Pau, K., Bowton, E., Speed, N., Lute, B. J., Anderson, M., Sen, N., Robertson, S. D., Vaughan, R. A., Rothman, J. E., Galli, A., Javitch, J. A., and Yamamoto, A. (2011) Flotillin-1 is essential for PKC-triggered endocytosis and membrane microdomain localization of DAT. *Nat. Neurosci. 14* (4), 469−477.

(13) Binda, F., Dipace, C., Bowton, E., Robertson, S. D., Lute, B. J., Fog, J. U., Zhang, M., Sen, N., Colbran, R. J., Gnegy, M. E., Gether, U., Javitch, J. A., Erreger, K., and Galli, A. (2008) Syntaxin 1A interaction with the dopamine transporter promotes amphetamine-induced dopamine efflux. *Mol. Pharmacol. 74* (4), 1101−1108.

(14) Bjerggaard, C., Fog, J. U., Hastrup, H., Madsen, K., Loland, C. J., Javitch, J. A., and Gether, U. (2004) Surface Targeting of the Dopamine Transporter Involves Discrete Epitopes in the Distal C Terminus But Does Not Require Canonical PDZ Domain Interactions. *J. Neurosci. 24* (31), 7024−7036.

(15) Boudanova, E., Navaroli, D. M., Stevens, Z., and Melikian, H. E. (2008) Dopamine transporter endocytic determinants: carboxy terminal residues critical for basal and PKC-stimulated internalization. *Mol. Cell. Neurosci. 39* (2), 211−217.

(16) Bowton, E., Saunders, C., Erreger, K., Sakrikar, D., Matthies, H. J., Sen, N., Jessen, T., Colbran, R. J., Caron, M. G., Javitch, J. A., Blakely, R. D., and Galli, A. (2010) Dysregulation of dopamine transporters via dopamine D2 autoreceptors triggers anomalous dopamine efflux associated with attention-deficit hyperactivity disorder. *J. Neurosci. 30* (17), 6048−6057.

(17) Fog, J. U., Khoshbouei, H., Holy, M., Owens, W. A., Vaegter, C. B., Sen, N., Nikandrova, Y., Bowton, E., McMahon, D. G., Colbran, R. J., Daws, L. C., Sitte, H. H., Javitch, J. A., Galli, A., and Gether, U. (2006) Calmodulin kinase II interacts with the dopamine transporter C terminus to regulate amphetamine-induced reverse transport. *Neuron 51* (4), 417−429.

(18) Foster, J. D., Adkins, S. D., Lever, J. R., and Vaughan, R. A. (2008) Phorbol ester induced trafficking-independent regulation and enhanced phosphorylation of the dopamine transporter associated with membrane rafts and cholesterol. *J. Neurochem. 105* (5), 1683−1699.

(19) Foster, J. D., and Vaughan, R. A. (2011) Palmitoylation controls dopamine transporter kinetics, degradation, and protein kinase C-dependent regulation. *J. Biol. Chem. 286* (7), 5175−5186.

(20) Hong, W. C., and Amara, S. G. (2010) Membrane cholesterol modulates the outward facing conformation of the dopamine transporter and alters cocaine binding. *J. Biol. Chem. 285* (42), 32616−32626.

(21) Navaroli, D. M., Stevens, Z. H., Uzelac, Z., Gabriel, L., King, M. J., Lifshitz, L. M., Sitte, H. H., and Melikian, H. E. (2011) The plasma membrane-associated GTPase Rin interacts with the dopamine transporter and is required for protein kinase C-regulated dopamine transporter trafficking. *J. Neurosci. 31* (39), 13758−13770.

(22) Saunders, C., Ferrer, J. V., Shi, L., Chen, J., Merrill, G., Lamb, M. E., Leeb-Lundberg, L. M. F., Carvelli, L., Javitch, J. A., and Galli, A. (2000) Amphetamine-induced loss of human dopamine transporter activity: An internalization-dependent and cocaine-sensitive mechanism. *Proc. Natl. Acad. Sci. U. S. A. 97* (12), 6850−6855.

(23) Torres, G. E., Carneiro, A., Seamans, K., Fiorentini, C., Sweeney, A., Yao, W.-D., and Caron, M. G. (2003) Oligomerization and Trafficking of the Human Dopamine Transporter Mutational Analysis Identifies Critical Domains Important for the Functional Expression of the Transporter. *J. Biol. Chem. 278* (4), 2731−2739.

(24) Adkins, E. M., Samuvel, D. J., Fog, J. U., Eriksen, J., Jayanthi, L. D., Vaegter, C. B., Ramamoorthy, S., and Gether, U. (2007) Membrane Mobility and Microdomain Association of the Dopamine Transporter Studied with Fluorescence Correlation Spectroscopy and Fluorescence Recovery after Photobleaching. *Biochemistry 46* (37), 10484−10497.

(25) Furman, C. A., Chen, R., Guptaroy, B., Zhang, M., Holz, R. W., and Gnegy, M. (2009) Dopamine and amphetamine rapidly increase dopamine transporter trafficking to the surface: live-cell imaging using total internal reflection fluorescence microscopy. *J. Neurosci. 29* (10), 3328−3336.

(26) Eriksen, J., Rasmussen, S. G., Rasmussen, T. N., Vaegter, C. B., Cha, J. H., Zou, M. F., Newman, A. H., and Gether, U. (2009) Visualization of dopamine transporter trafficking in live neurons by use of fluorescent cocaine analogs. *J. Neurosci. 29* (21), 6794−6808.

(27) Sakrikar, D., Mazei-Robison, M. S., Mergy, M. A., Richtand, N. W., Han, Q., Hamilton, P. J., Bowton, E., Galli, A., Veenstra-VanderWeele, J., Gill, M., and Blakely, R. D. (2012) Attention Deficit/Hyperactivity Disorder-Derived Coding Variation in the Dopamine Transporter Disrupts Microdomain Targeting and Trafficking Regulation. *J. Neurosci. 32* (16), 5385−5397.

(28) Bruchez, M., Jr., Moronne, M., Gin, P., Weiss, S., and Alivisatos, A. P. (1998) Semiconductor Nanocrystals as Fluorescent Biological Labels. *Science 281* (5385), 2013−2016.

DOI: 10.1021/cn500202c
ACS Chem. Neurosci. 2015, 6, 526−534

(29) Chan, W. C. W, and Nie, S. (1998) Quantum Dot Bioconjugates for Ultrasensitive Nonisotopic Detection. *Science 281* (5385), 2016−2018.
(30) Rosenthal, S. J., Chang, J. C., Kovtun, O., McBride, J. R., and Tomlinson, I. D. (2011) Biocompatible Quantum Dots for Biological Applications. *Chem. Biol. 18* (1), 10−24.
(31) Dahan, M., Lévi, S., Luccardini, C., Rostaing, P., Riveau, B., and Triller, A. (2003) Diffusion dynamics of glycine receptors revealed by single-quantum dot tracking. *Science 302* (5644), 442−445.
(32) Pinaud, F., Clarke, S., Sittner, A., and Dahan, M. (2010) Probing cellular events, one quantum dot at a time. *Nat. Methods 7* (4), 275−285.
(33) Rosenthal, S. J., Tomlinson, I., Adkins, E. M., Schroeter, S., Adams, S., Swafford, L., McBride, J., Wang, Y., DeFelice, L. J., and Blakely, R. D. (2002) Targeting Cell Surface Receptors with Ligand-Conjugated Nanocrystals. *J. Am. Chem. Soc. 124* (17), 4586−4594.
(34) Tomlinson, I. D., Mason, J., Burton, J. N., Blakely, R. D., and Rosenthal, S. J. (2003) The design and synthesis of novel derivatives of the dopamine uptake inhibitors GBR 12909 and GBR 12935. High-affinity dopaminergic ligands for conjugation with highly fluorescent cadmium selenide/zinc sulfide core/shell nanocrystals. *Tetrahedron 59* (40), 8035−8047.
(35) Tomlinson, I. D., Mason, J. N., Blakely, R. D., and Rosenthal, S. J. (2006) High affinity inhibitors of the dopamine transporter (DAT): Novel biotinylated ligands for conjugation to quantum dots. *Bioorg. Med. Chem. Lett. 16* (17), 4664−4667.
(36) Tomlinson, I. D., Mason, J. N., Blakely, R. D., and Rosenthal, S. J. (2005) Inhibitors of the serotonin transporter protein (SERT): The design and synthesis of biotinylated derivatives of 3-(1,2,3,6-tetrahydro-pyridin-4-yl)-1H-indoles. High-affinity serotonergic ligands for conjugation with quantum dots. *Bioorg. Med. Chem. Lett. 15* (23), 5307−5310.
(37) Tomlinson, I. D., Iwamoto, H., Blakely, R. D., and Rosenthal, S. J. (2011) Biotin tethered homotryptamine derivatives: High affinity probes of the human serotonin transporter (hSERT). *Bioorg. Med. Chem. Lett. 21* (6), 1678−1682.
(38) Kovtun, O., Tomlinson, I. D., Sakrikar, D. S., Chang, J. C., Blakely, R. D., and Rosenthal, S. J. (2011) Visualization of the Cocaine-Sensitive Dopamine Transporter with Ligand-Conjugated Quantum Dots. *ACS Chem. Neurosci. 2* (7), 370−378.
(39) Chang, J. C., Tomlinson, I. D., Warnement, M. R., Iwamoto, H., DeFelice, L. J., Blakely, R. D., and Rosenthal, S. J. (2011) A Fluorescence Displacement Assay for Antidepressant Drug Discovery Based on Ligand-Conjugated Quantum Dots. *J. Am. Chem. Soc. 133* (44), 17528−17531.
(40) Kovtun, O., Ross, E. J., Tomlinson, I. D., and Rosenthal, S. J. (2012) A flow cytometry-based dopamine transporter binding assay using antagonist-conjugated quantum dots. *J. Chem. Soc., Chem. Commun. 48* (44), 5428−5430.
(41) Chang, J. C., Tomlinson, I. D., Warnement, M. R., Ustione, A., Carneiro, A. M. D., Piston, D. W., Blakely, R. D., and Rosenthal, S. J. (2012) Single Molecule Analysis of Serotonin Transporter Regulation Using Antagonist-Conjugated Quantum Dots Reveals Restricted, p38 MAPK-Dependent Mobilization Underlying Uptake Activation. *J. Neurosci. 32*, 8919−8929.
(42) Nirmal, M.; Brus, L. (1999) Luminescence Photophysics in Semiconductor Nanocrystals. *Acc. Chem. Res. 32*, 407−414.
(43) Kuno, M., Fromm, D. P., Hamann, H. F., Gallagher, A., and Nesbitt, D. J. (2000) Nonexponential blinking" kinetics of single CdSe quantum dots: A universal power law behavior. *J. Chem. Phys. 112* (7), 3117−3120.
(44) Neuhauser, R. G., Shimizu, K. T., Woo, W. K., Empedocles, S. A., and Bawendi, M. G. (2000) Correlation between Fluorescence Intermittency and Spectral Diffusion in Single Semiconductor Quantum Dots. *Phys. Rev. Lett. 85* (15), 3301−3304.
(45) Frantsuzov, P., Kuno, M., Janko, B., and Marcus, R. A. (2008) Universal emission intermittency in quantum dots, nanorods and nanowires. *Nat. Phys. 4* (5), 519−522.
(46) Bentzen, E. L., Tomlinson, I. D., Mason, J., Gresch, P., Warnement, M. R., Wright, D., Sanders-Bush, E., Blakely, R., and Rosenthal, S. J. (2005) Surface Modification To Reduce Nonspecific Binding of Quantum Dots in Live Cell Assays. *Bioconjugate Chem. 16* (6), 1488−1494.
(47) Chang, J. C., and Rosenthal, S. J. (2012) Visualization of Lipid Raft Membrane Compartmentalization in Living RN46A Neuronal Cells Using Single Quantum Dot Tracking. *ACS Chem. Neurosci. 3*, 737−743.
(48) Vrljic, M., Nishimura, S. Y., and Moerner, W. E. (2007) Single-Molecule Tracking. *Methods Mol. Biol. 398*, 193−219.
(49) Martin, D. S., Forstner, M. B., and Kas, J. A. (2002) Apparent subdiffusion inherent to single particle tracking. *Biophys. J. 83*, 2109−2117.
(50) Daumas, F., Destainville, N., Millot, C., Lopez, A., Dean, D., and Salome, L. (2003) Confined diffusion without fences of a g-protein-coupled receptor as revealed by single particle tracking. *Biophys. J. 84*, 356−366.
(51) Lingwood, D., and Simons, K. (2010) Lipid rafts as a membrane-organizing principle. *Science 327*, 46−50.
(52) Simons, K., and Toomre, D. (2000) Lipid rafts and signal transduction. *Nat. Rev. Mol. Cell Biol. 1*, 31−40.
(53) Brown, D. A., and London, E. (1998) Functions of lipid rafts in biological membranes. *Annu. Rev. Cell Dev. Biol. 14*, 111−136.
(54) Torres, G. E., Yao, W.-D., Mohn, A. R., Quan, H., Kim, K.-M., Levey, A. I., Staudinger, J., and Caron, M. G. (2001) Functional Interaction between Monoamine Plasma Membrane Transporters and the Synaptic PDZ Domain−Containing Protein PICK1. *Neuron 30* (1), 121−134.
(55) Bjerggaard, C., Fog, J. U., Hastrup, H., Madsen, K., Loland, C. J., Javitch, J. A., and Gether, U. (2004) Surface targeting of the dopamine transporter involves discrete epitopes in the distal C terminus but does not require canonical PDZ domain interactions. *J. Neurosci. 24* (31), 7024−7036.
(56) Rao, A., Richards, T. L., Simmons, D., Zahniser, N. R., and Sorkin, A. (2012) Epitope-tagged dopamine transporter knock-in mice reveal rapid endocytic trafficking and filopodia targeting of the transporter in dopaminergic axons. *FASEB J. 26* (5), 1921−1933.
(57) Kusumi, A., Sako, Y., and Yamamoto, M. (1993) Confined lateral diffusion of membrane receptors as studied by single particle tracking (nanovid microscopy). Effects of calcium-induced differentiation in cultured epithelial cells. *Biophys. J. 65*, 2021−2040.
(58) Triller, A., and Choquet, D. (2008) New concepts in synaptic biology derived from single-molecule imaging. *Neuron 59*, 359−374.
(59) Medintz, I. L., Uyeda, H. T., Goldman, E. R., and Mattoussi, H. (2005) Quantum dot bioconjugates for imaging, labelling and sensing. *Nat. Mater. 4* (6), 435−446.
(60) Toulme, E., and Khakh, B. S. (2012) Imaging P2 × 4 Receptor Lateral Mobility in Microglia: Regulation by Calcium and p38 MAPK. *J. Biol. Chem. 287* (18), 14734−14748.
(61) Gomez-Varela, D., and Berg, D. K. (2013) Lateral Mobility of Presynaptic α7-Containing Nicotinic Receptors and Its Relevance for Glutamate Release. *J. Neurosci. 33* (43), 17062−17071.
(62) Murphy-Royal, C., Dupuis, J. P., Varela, J. A., Panatier, A., Pinson, B., Baufreton, J., Groc, L., and Oliet, S. H. R. (2015) Surface diffusion of astrocytic glutamate transporters shapes synaptic transmission. *Nat. Neurosci. 18* (2), 219−226.

DOI: 10.1021/cn500202c
ACS Chem. Neurosci. 2015, 6, 526−534